

## Electronic Supplementary Information

### **A Facile approach to prepare silica hybrid, spin crossover water-soluble nanoparticles as a potential platform for thermally responsive MRI agents**

Patroula Gkolfi,<sup>a</sup> Dimitra Tsivaka,<sup>b</sup> Ioannis Tsougos,<sup>\*b</sup> Katerina Vassiou,<sup>c</sup> Ondřej Malina,<sup>\*d</sup> Michaela Polaskova,<sup>d,e</sup> Christina D. Polyzou,<sup>\*a</sup> Christos T. Chasapis<sup>f</sup> and Vassilis Tangoulis<sup>\*a</sup>

<sup>a</sup>*Department of Chemistry, Laboratory of Inorganic Chemistry, University of Patras, 26504, Patras, Greece. Email: [chpolyzou@upatras.gr](mailto:chpolyzou@upatras.gr) and [vtango@upatras.gr](mailto:vtango@upatras.gr)*

<sup>b</sup>*Department of Medical Physics, University Hospital of Larissa, University of Thessaly, Biopolis, GR-41110 Larissa, Greece*

<sup>c</sup>*Department of Radiology, University Hospital of Larissa, University of Thessaly, Biopolis, GR-41110 Larissa, Greece*

<sup>d</sup>*Regional Centre of Advanced Technologies and Materials, Departments of Physical Chemistry and Experimental Physics, Faculty of Science, Palacký University Olomouc, Šlechtitelů 27, 783 71 Olomouc, Czech Republic. Email: [ondrej.malina@upol.cz](mailto:ondrej.malina@upol.cz)*

<sup>e</sup>*Department of Experimental Physics, Faculty of Science, Palacký University Olomouc, 17. Listopadu 1192/12, 771 46 Olomouc, Czech Republic*

<sup>f</sup>*NMR Facility, Instrumental Analysis Laboratory, School of Natural Sciences, University of Patras, 26504, Patras, Greece*

<i>EXPERIMENTAL SECTION</i>	<b>3</b>
<i>PHYSICAL MEASUREMENTS</i>	<b>5</b>
• Elemental Analysis	<b>6</b>
• EDS Analysis	<b>6</b>
• FT-Infrared Spectroscopy	<b>7</b>
• X-ray Powder Diffraction	<b>8</b>
• HR-TEM Microscopy	<b>14</b>
• UV-Vis Spectroscopy	<b>16</b>
• Dynamic Light Scattering	<b>18</b>
• Differential Scanning Calorimetry	<b>20</b>
• Magnetic Resonance Imaging	<b>21</b>

## Experimental Section

### Materials

All manipulations were performed under aerobic conditions using reagents and solvents (Alfa Aesar, Sigma Aldrich, Serva) as received. The ligands 1H-1,2,4-triazole (HTrz), 4-amino-4H-1,2,4-triazole (NH<sub>2</sub>trz), the tetraethoxysilane (TEOS) and (3-aminopropyl)triethoxysilane (APTES) were purchased from Alfa-Aesar, while the iron(II)tetrafluoroborate hexahydrate salt, Fe(BF<sub>4</sub>)<sub>2</sub>·6H<sub>2</sub>O and n-hexanol from Sigma Aldrich. Triton X-100 and cyclohexane were obtained from Serva used without further purification. The deionized water used for synthesis was deoxygenated by simultaneous sonication and argon bubbling during 1 h.

### Synthesis of NPs

**NPs 1.** An aqueous solution of Fe(BF<sub>4</sub>)<sub>2</sub>·6H<sub>2</sub>O (337 mg, 1.00 mmol) in 0.5 mL of deionized H<sub>2</sub>O and 0.1 mL of TEOS were added to a solution containing Triton X-100 (1.8 mL), n-hexanol (1.8 mL) and cyclohexane (7.5 mL). The resulting mixture was stirred for 30 min until the formation of a clear water-in-oil microemulsion. A similar procedure was applied to 1,2,4,1*H*-Triazole (HTrz) (210 mg, 3.00 mmol) in 0.5 mL of deionized H<sub>2</sub>O. Both microemulsions were quickly combined and the mixture was stirred for 24 h in the dark until the addition of 100 μL APTES. After 30 min of stirring 100 μL TEOS were added and the stirring continued for further 24 h followed by the addition of acetone to break the microemulsion. The precipitated nanoparticles were isolated by centrifugation at 6000 rpm, washed several times with EtOH, then acetone and finally dried under vacuum.

**NPs 2.** An aqueous solution of Fe(BF<sub>4</sub>)<sub>2</sub>·6H<sub>2</sub>O (337 mg, 1.00 mmol) and ascorbic acid (35 mg, 0.20 mmol) in 0.5 mL of deionized H<sub>2</sub>O and 0.1 mL of TEOS were added to a solution containing Triton X-100 (1.8 mL), n-hexanol (1.8 mL) and cyclohexane (7.5 mL). The resulting mixture was stirred for 30 min until the formation of a clear water-in-oil microemulsion. A similar procedure was applied to 1,2,4,1*H*-Triazole (HTrz) (199 mg, 2.90 mmol) and 4-amino-1,2,4-triazole (NH<sub>2</sub>Trz) (8 mg, 0.10 mmol) in 0.5 mL of deionized H<sub>2</sub>O. Both microemulsions were quickly combined and the mixture was stirred for 24 h in the dark until the addition of 100 μL APTES. After 30 min of stirring 100 μL TEOS were added and the stirring continued for further 24 h followed by the addition of acetone to break the microemulsion. The precipitated nanoparticles were

isolated by centrifugation at 6000 rpm, washed several times with EtOH, then acetone and finally dried under vacuum.

**NPs 3.** An aqueous solution of  $\text{Fe}(\text{BF}_4)_2 \cdot 6\text{H}_2\text{O}$  (304 mg, 0.90 mmol),  $\text{Zn}(\text{BF}_4)_2 \cdot 6\text{H}_2\text{O}$  (35 mg, 0.10 mmol) and ascorbic acid (35 mg, 0.20 mmol) in 0.5 mL of deionized  $\text{H}_2\text{O}$  and 0.1 mL of TEOS were added to a solution containing Triton X-100 (1.8 mL), n-hexanol (1.8 mL) and cyclohexane (7.5 mL). The resulting mixture was stirred for 30 min until the formation of a clear water-in-oil microemulsion. A similar procedure was applied to 1,2,4,1*H*-Triazole (HTrz) (199 mg, 2.90 mmol) and 4-amino-1,2,4-triazole ( $\text{NH}_2\text{Trz}$ ) (8 mg, 0.10 mmol) in 0.5 mL of deionized  $\text{H}_2\text{O}$ . Both microemulsions were quickly combined and the mixture was stirred for 24 h in the dark until the addition of 100  $\mu\text{L}$  APTES. After 30 min of stirring 100  $\mu\text{L}$  TEOS were added and the stirring continued for further 24 h followed by the addition of acetone to break the microemulsion. The precipitated nanoparticles were isolated by centrifugation at 6000 rpm, washed several times with EtOH, then acetone and finally dried under vacuum.

**NPs 4.** An aqueous solution of  $\text{Fe}(\text{BF}_4)_2 \cdot 6\text{H}_2\text{O}$  (337 mg, 1.00 mmol) and ascorbic acid (35 mg, 0.20 mmol) in 0.5 mL of deionized  $\text{H}_2\text{O}$  and 0.1 mL of TEOS were added to a solution containing Triton X-100 (1.8 mL), n-hexanol (1.8 mL) and cyclohexane (7.5 mL). The resulting mixture was stirred for 30 min until the formation of a clear water-in-oil microemulsion. A similar procedure was applied to 1,2,4,1*H*-Triazole (HTrz) (185 mg, 2.70 mmol) and 4-amino-1,2,4-triazole ( $\text{NH}_2\text{Trz}$ ) (25 mg, 0.30 mmol) in 0.5 mL of deionized  $\text{H}_2\text{O}$ . Both microemulsions were quickly combined and the mixture was stirred for 24 h in the dark until the addition of 100  $\mu\text{L}$  APTES. The stirring continued for 30 min and then addition of acetone was followed in order to break the microemulsion. The precipitated nanoparticles were isolated by centrifugation at 6000 rpm, washed several times with EtOH, then acetone and finally dried under vacuum.

## PHYSICAL MEASUREMENTS

Elemental analyses (C, H, N) were performed by the in-house facilities of the University of Patras (Greece). IR spectra ( $4000\text{--}400\text{ cm}^{-1}$ ) were recorded using a Perkin-Elmer 16PC FT-IR spectrometer with samples prepared as KBr pellets. UV-Vis absorption spectra were recorded between 280 and 1100 nm by using the spectrometer PGS-2 produced by Carl Zeiss. The powder X-ray diffraction (PXRD) measurements were performed at room temperature on a Malvern Panalytical X'Pert PRO diffractometer with focusing  $\text{K}\alpha_1$  geometry. Polycrystalline samples were loaded in 1 mm borosilicate glass capillaries while the X-ray tube operated at 45 kV and 40 mA. The incident-beam side ( $\text{CuK}\alpha_1$  radiation,  $\lambda = 1.54056\text{ \AA}$ ) is equipped with a focusing X-ray mirror, a 0.5° fixed divergence slit, 0.5° anti-scatter slits and 0.04 rad Soller slits, while on the diffracted-beam side the system was configured with 0.04 rad Soller slits and a PIXcel1D detector with anti-scatter shielding. Four scans were performed in Debye-Scherrer mode, with a step size of 0.0066° on a spinning stage (~300 rpm), within a  $2\theta$  range of 4.0–90.0°. No radiation damage was observed even after 5 h of measurement, therefore all scans were merged together to increase counting statistics. TEM study performed utilizing a FEI CM20 TEM operating at 200 kV. TEM specimens prepared by drop casting a 3  $\mu\text{L}$  droplet of nanoparticles suspension in acetone on a carbon coated Cu TEM grid. The size of the particles determined by “manual counting” using ImageJ software (<https://imagej.net>). The direct-current (DC) magnetic susceptibility measurements were measured on powder samples using a physical-properties measurement system (PPMS, Quantum Design) at 2 – 300 K with a rate of 0.5 K  $\text{min}^{-1}$  under an applied dc magnetic field of 1000 Oe. The experimental data were corrected for the diamagnetism and signal of the sample holder and the Pascal constants were used for the diamagnetic corrections. Differential Scanning Calorimetry (DSC) measurements were carried out in a N-(g) atmosphere using a DSC (Q100, TA Instruments, USA) instrument. Aluminium hermetic pans were used to encapsulate 5–7 mg of sample. The pans were purged with nitrogen at a rate of 50  $\text{mL}\cdot\text{min}^{-1}$  and liquid nitrogen was used for cooling. Initially, the samples were cooled down from 200 K to 450 K at the maximum permissible rate by the instrument. Then the samples were subjected to two successive thermal regimes; (a) heating from 200 K to 450 K at a rate of 1 K  $\text{min}^{-1}$  and (b) cooling to 200 K at the same rate. At the beginning and end of each heating and cooling run the sample was held isothermally for 5 min. DLS measurements were performed using a ZetaSizer Zen3600 (Malvern Instruments). The sample was loaded into a disposable micro cuvette and measured at 25 °C. The intensity size distribution or the Z-average diameter was obtained using the cumulant analysis with a repeatability of 1.6%.

To sum up, physical and structural characterization of the NPs was carried out with Infrared (IR) Spectroscopy and X-ray Powder Diffraction (p-XRD), while Differential Scanning Calorimetry (DSC) studies were also applied for each case in order to determine the SCO behavior in solid state. Transmission Electron Microscopy (TEM) was used to define the shape and size of the NPs, while UV-Vis Spectroscopy (UV-Vis) and Dynamic Light Scattering (DLS) were used for gathering important data collection regarding the NPs behavior in their aqueous dispersions.

## Elemental Analyses

**Table S1.** Elemental analyses for NPs 1 - 4.

Sample		C [%]	N [%]	H [%]	Molecular Formulae
1	exptl	18.65	26.50	2.68	[Fe(Htrz) <sub>2</sub> (trz)](BF <sub>4</sub> )·1.4SiO <sub>2</sub> ·0.7H <sub>2</sub> O·0.4Acetone
	calcd	18.45	26.89	2.54	469 g/mol
2	exptl	16.81	24.50	2.44	[Fe(Htrz) <sub>2.1</sub> (trz) <sub>0.8</sub> (NH <sub>2</sub> trz) <sub>0.1</sub> ](BF <sub>4</sub> ) <sub>1.2</sub> ·1.9SiO <sub>2</sub> ·0.7H <sub>2</sub> O·0.4Acetone
	calcd	16.70	24.61	2.35	518 g/mol
3	exptl	16.78	27.87	2.23	[Fe <sub>0.9</sub> Zn <sub>0.1</sub> (Htrz) <sub>2.1</sub> (trz) <sub>0.8</sub> (NH <sub>2</sub> trz) <sub>0.1</sub> ](BF <sub>4</sub> ) <sub>1.2</sub> ·1.2SiO <sub>2</sub> ·0.4H <sub>2</sub> O·0.1Acetone
	calcd	16.67	28.08	2.15	455 g/mol
4	exptl	18.40	31.22	2.43	[Fe(Htrz) <sub>2</sub> (trz) <sub>0.7</sub> (NH <sub>2</sub> trz) <sub>0.3</sub> ](BF <sub>4</sub> ) <sub>1.3</sub> ·0.4SiO <sub>2</sub> ·0.3H <sub>2</sub> O·0.1Acetone
	calcd	18.24	31.39	2.38	415 g/mol

## EDS Analysis

Full scale counts: 2068

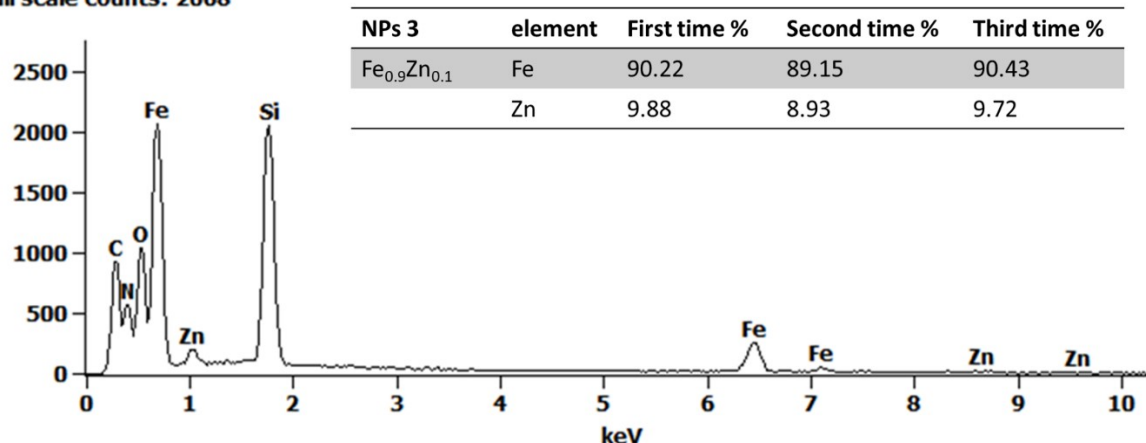


**Fig. S1.** Iron(II) and Zinc(II) ion content for the NPs 3 determined by energy dispersive spectroscopy (EDS) of field-emission scanning electron microscope (3<sup>rd</sup> time). In the inset there is a table depicting the ion contents for all the measurements.

## FT-IR Spectroscopy

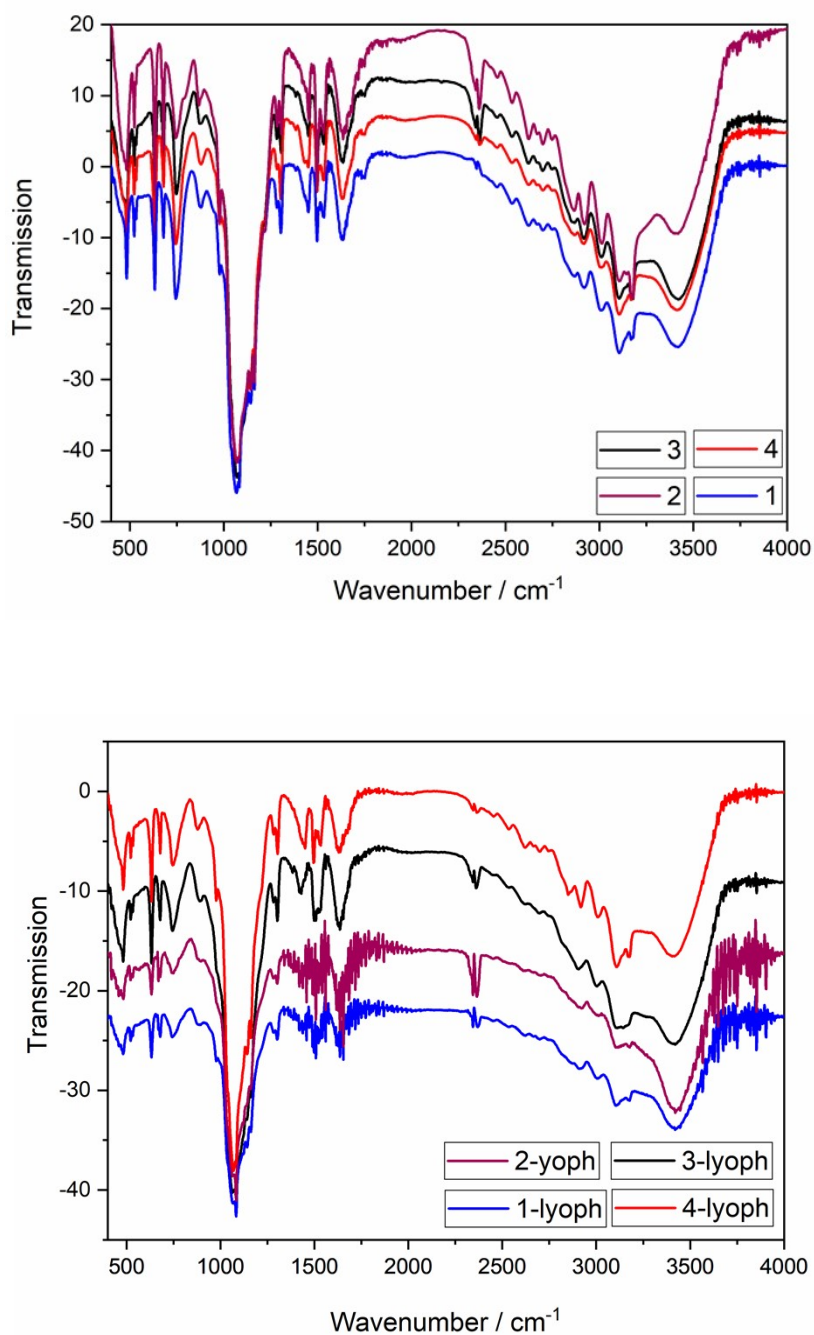
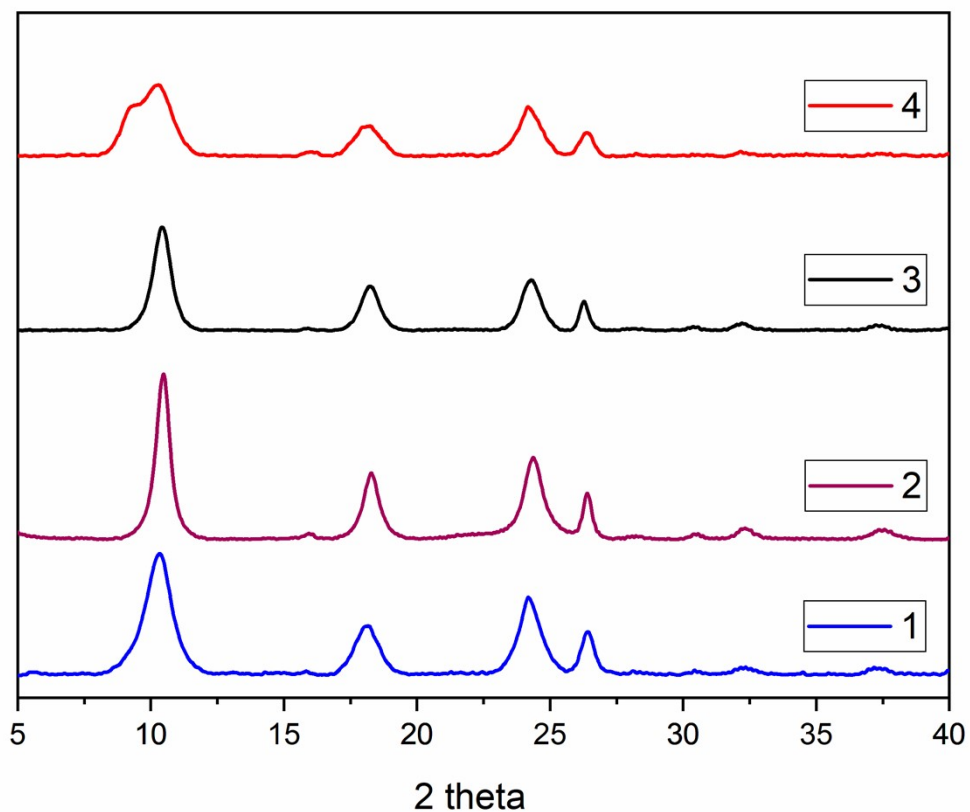


**Fig. S2.** IR spectra of the NPs **1 – 4** (a) and their lyophilized analogues (b).

Fig. S2 shows the FT-IR spectra of NPs **1 – 4**. In all cases the NPs exhibit similar features corresponding to the sharp peaks of SCO materials overlapped with characteristic peaks of SiO<sub>2</sub> coating. Several characteristic bands are at around 523 cm<sup>-1</sup>, 634 cm<sup>-1</sup> and 873 cm<sup>-1</sup> which attributed to the bending vibrations and out of plane stretching vibrations of the coordinated triazole ligand, while the bands at around 1221 cm<sup>-1</sup>, 1453 cm<sup>-1</sup> and 1496 cm<sup>-1</sup> correspond to the ring stretching. The bands at 483 cm<sup>-1</sup> and

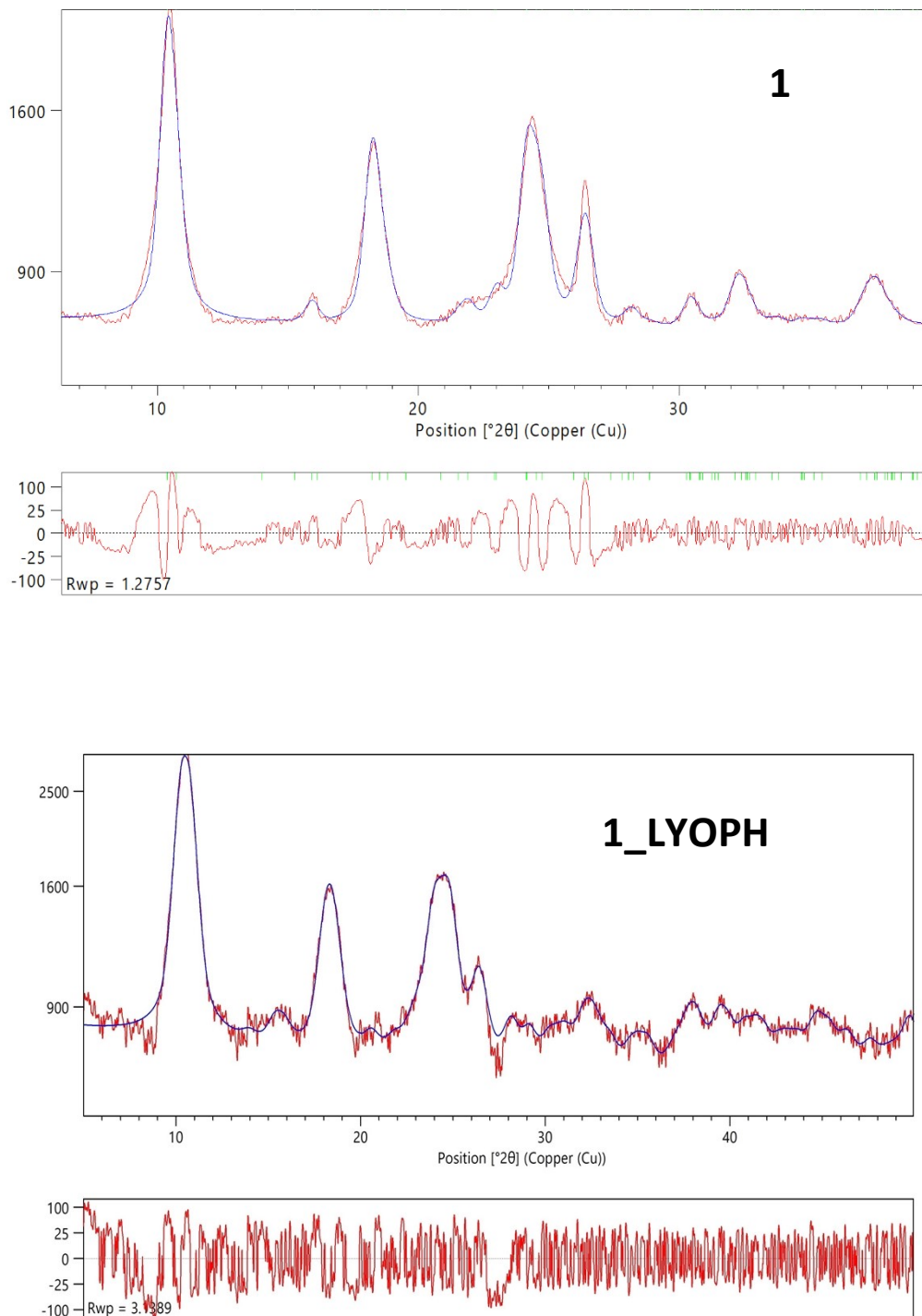
742  $\text{cm}^{-1}$  are probably attributed to two different types of bending vibrations for the Si-O-Si group, while the bands attributed to the  $\text{NH}_2$  groups are not easily distinct due to their overlapping with the triazole ligands.

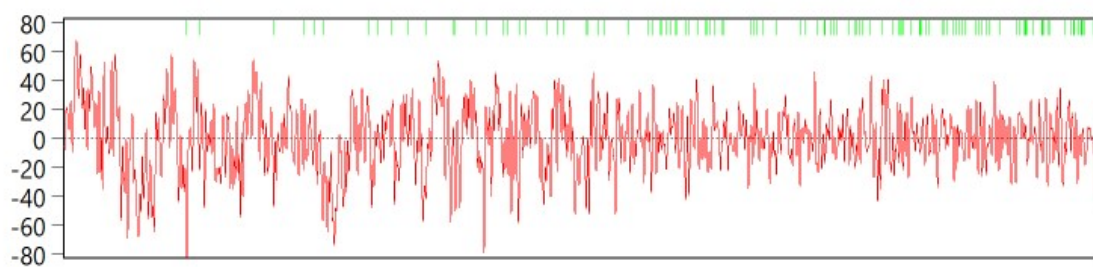
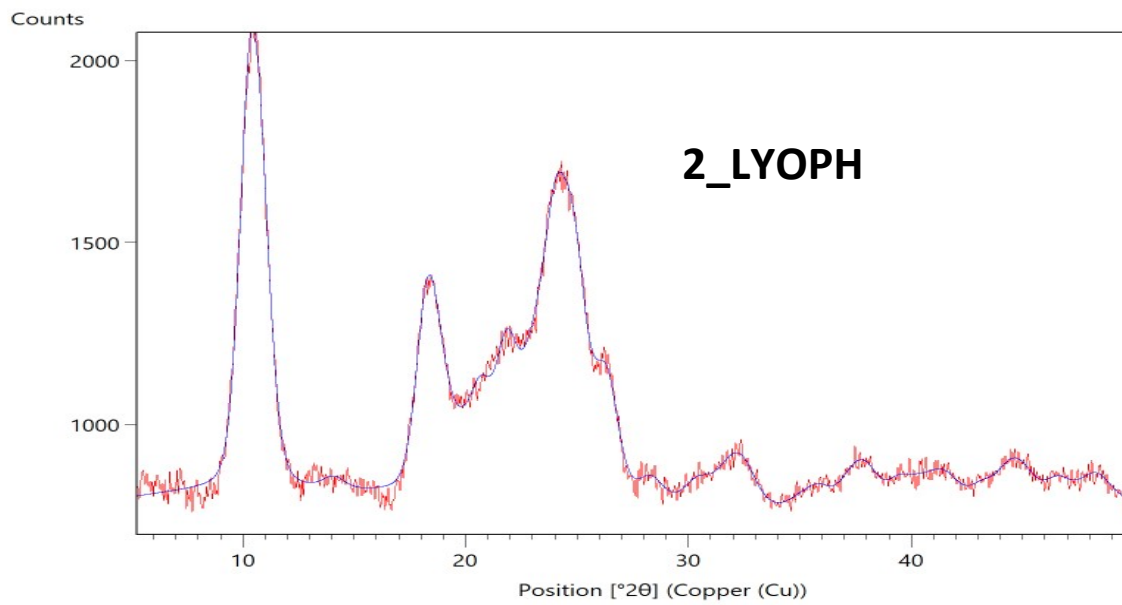
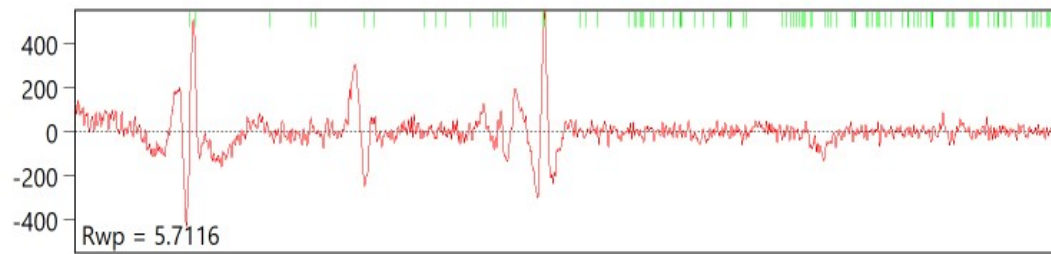
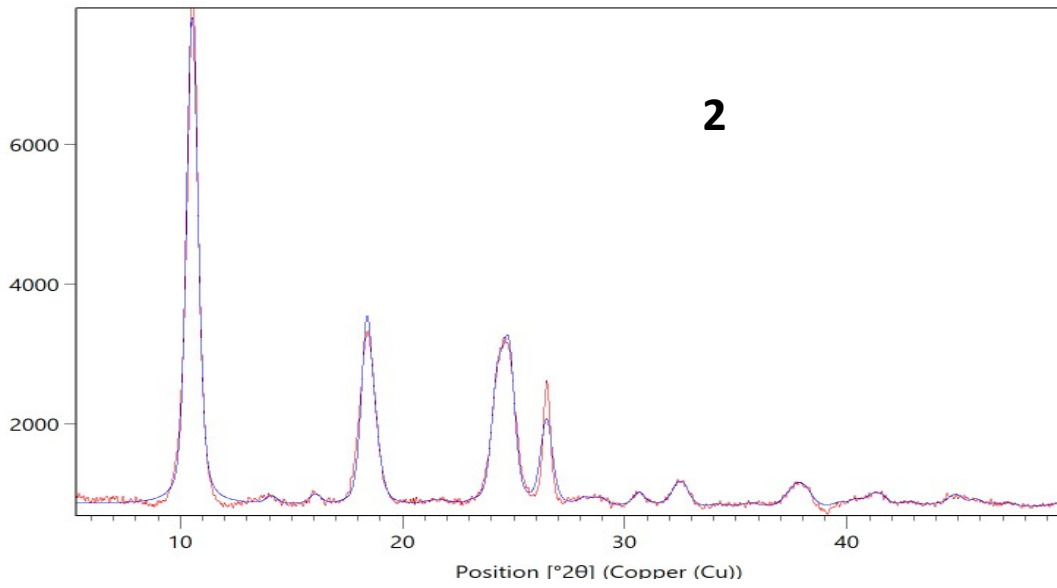
## X-ray Powder Diffraction

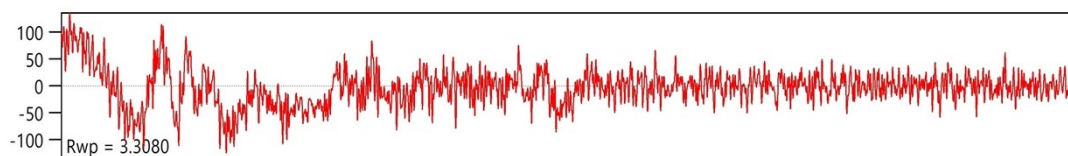
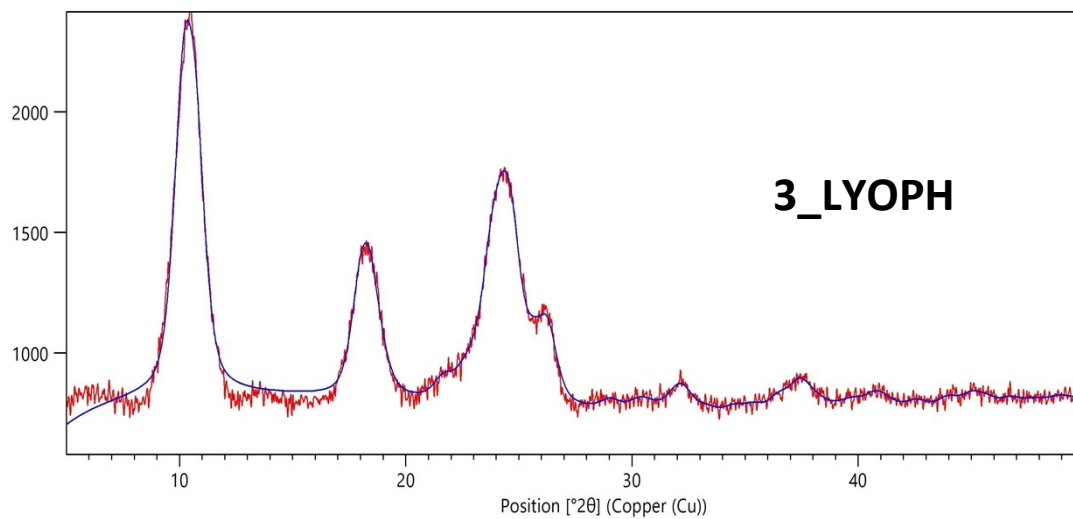
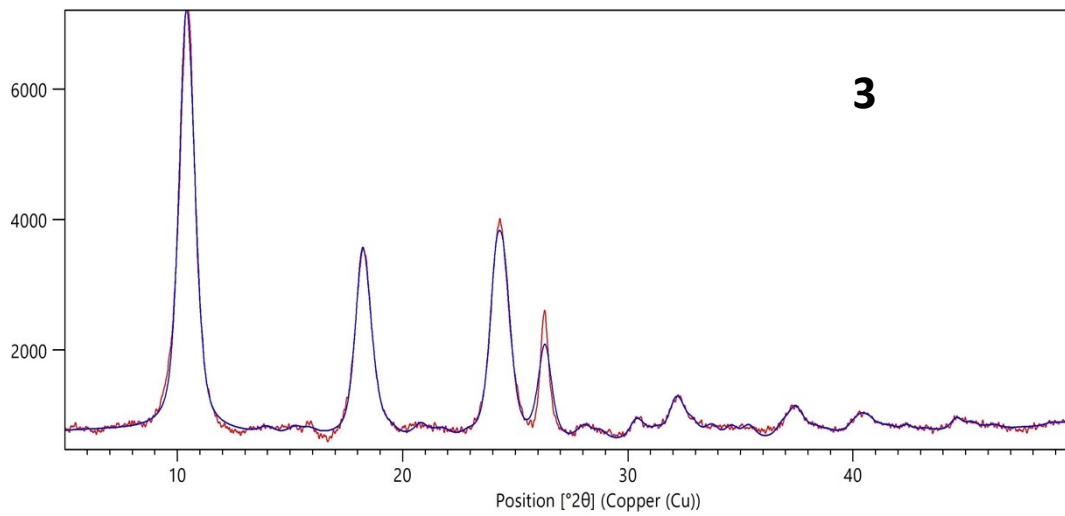


**Fig. S3a.** X-ray powder diffraction patterns for NPs **1 - 4**.

**Fig. S3b.** Pawley refinement plot of X-ray Diffraction data of NPs **1** - **4** and their lyophilized analogues 1 LYOPH – 4 LYOPH. Red line represents the experimental data, blue line is the calculated spectrum, and the lower spectrum represents the difference.







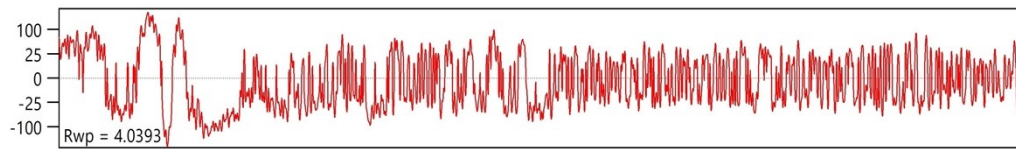
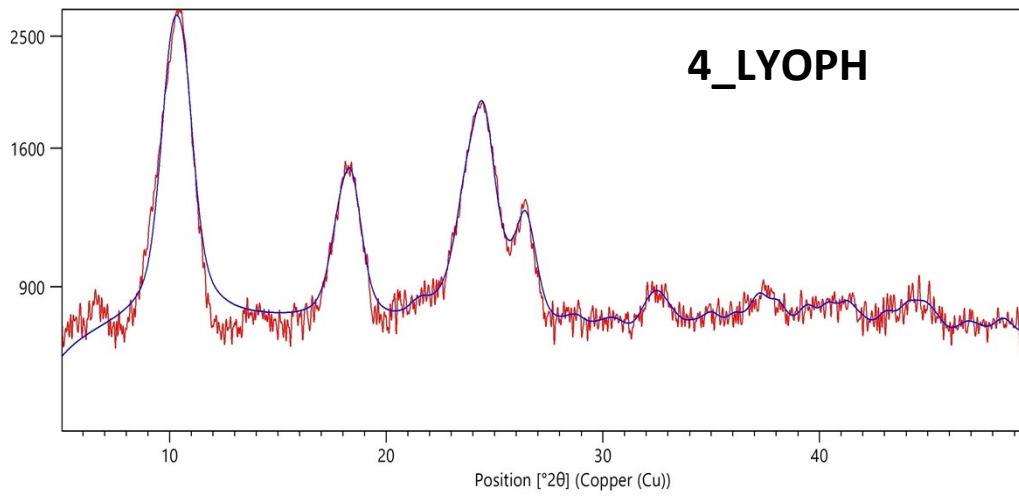
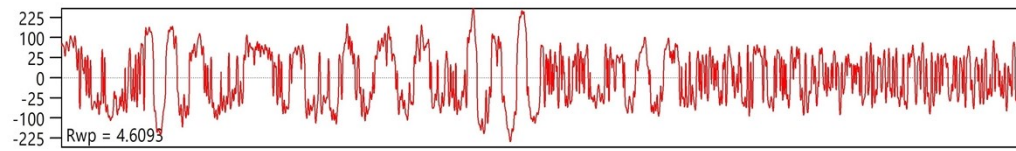
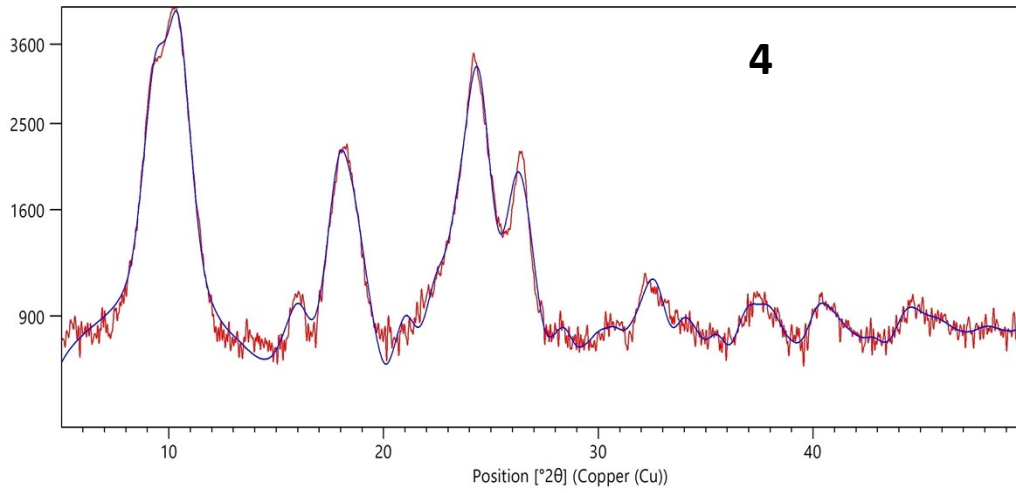


**Table S2.** Pawley refinement results of X-ray Diffraction data of NPs **1-4** and their Lyophilized analogues **1\_LYOPH – 4 LYOPH**

---

<i>NPs</i>	<i>a (Å)</i>	<i>b(Å)</i>	<i>c(Å)</i>	<i>V(Å<sup>3</sup>)</i>	<i>Crystallite Size(Å)</i>
<b>1</b>	17.0231	7.3533	9.4272	1180.1	261.1
<b>1_LYOPH</b>	17.2583	7.3298	9.3455	1182.2	137.3
<b>2</b>	16.9752	7.3512	9.4282	1167.1	272.1
<b>2_LYOPH</b>	17.1780	7.3545	9.2475	1168.9	200.3
<b>3</b>	17.0756	7.3791	9.4671	1192.8	154.9
<b>3_LYOPH</b>	17.4077	7.3674	9.3692	1201.6	127.5
<b>4</b>	17.3456	7.2940	9.5216	1208.8	100.6
<b>4_LYOPH</b>	17.5463	7.3062	9.4627	1213.1	116.5

# HR-TEM Microscopy

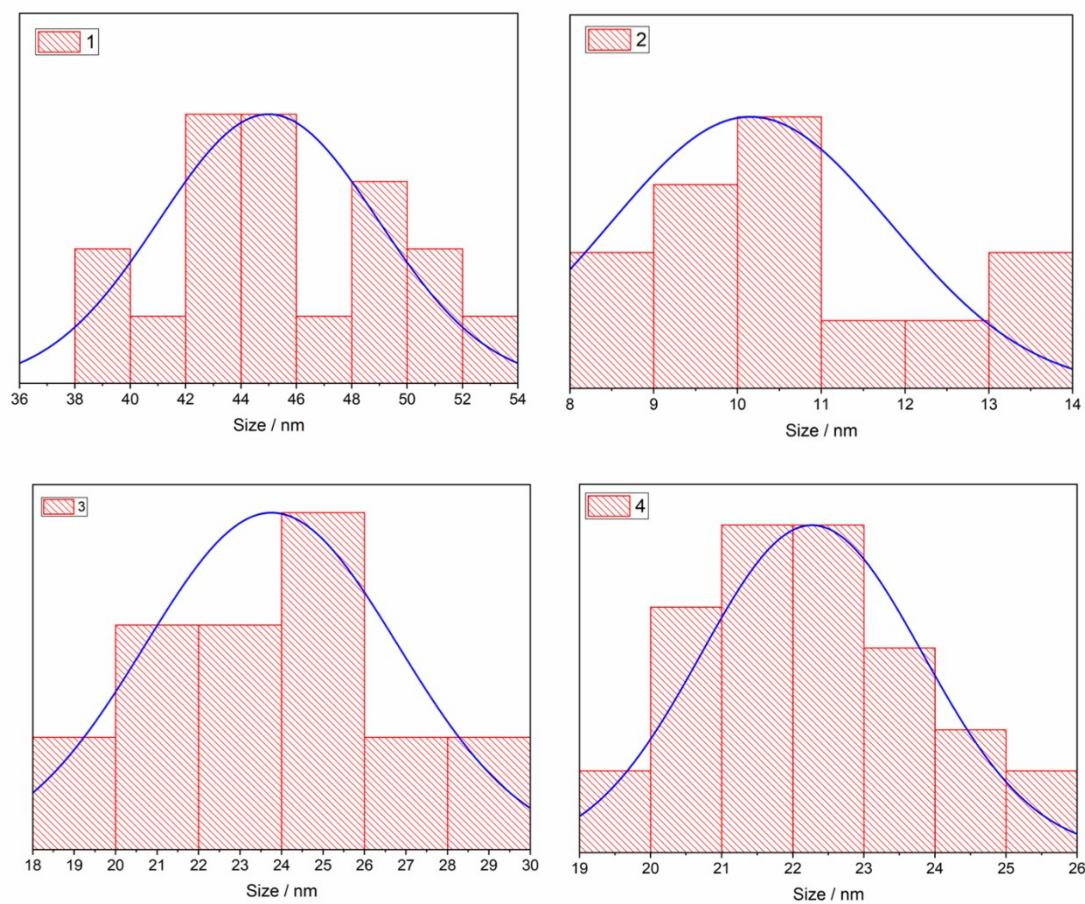


**Fig. S4.** Size distribution extracted from TEM images for NPs **1 - 4**.

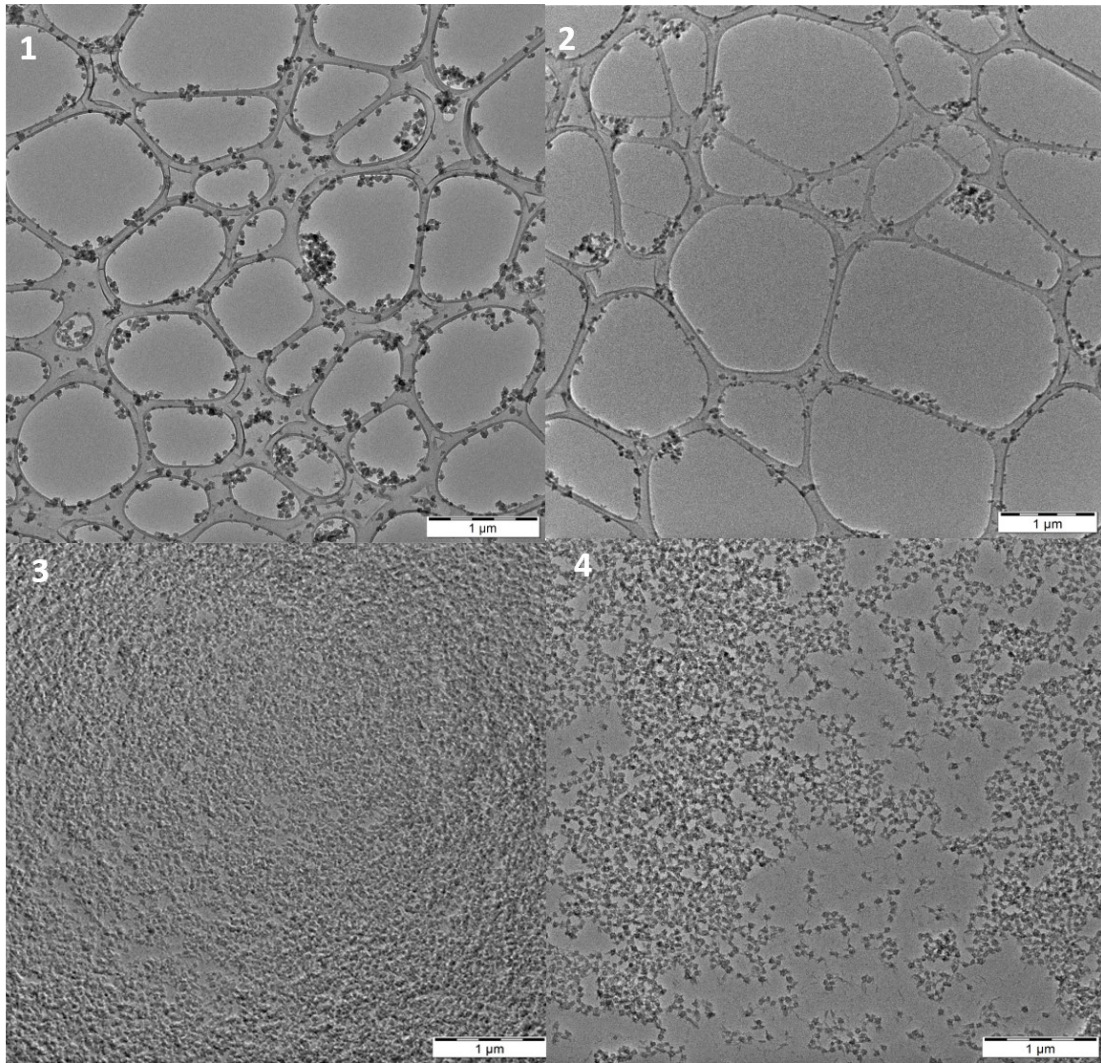


**Fig. S5.** TEM images for NPs 1 – 4 in 1 μm scale.

# UV-Vis Spectroscopy

**Table S3.** Time duration ( $t_0-t$ ) of the SCO phenomenon (evolution from LS to HS state) for the NPs **1 – 4** in aqueous dispersions according to UV-Vis Spectroscopy.

	2 mg dispersed in 5 mL H <sub>2</sub> O	Sample Dispersion at RT	Sample Thawing (from -20 °C to RT)
<b>1</b>		20 min	20 min
<b>2</b>		5 min	5 min
<b>3</b>		13 min	6 min
<b>4</b>		8 min	5 min

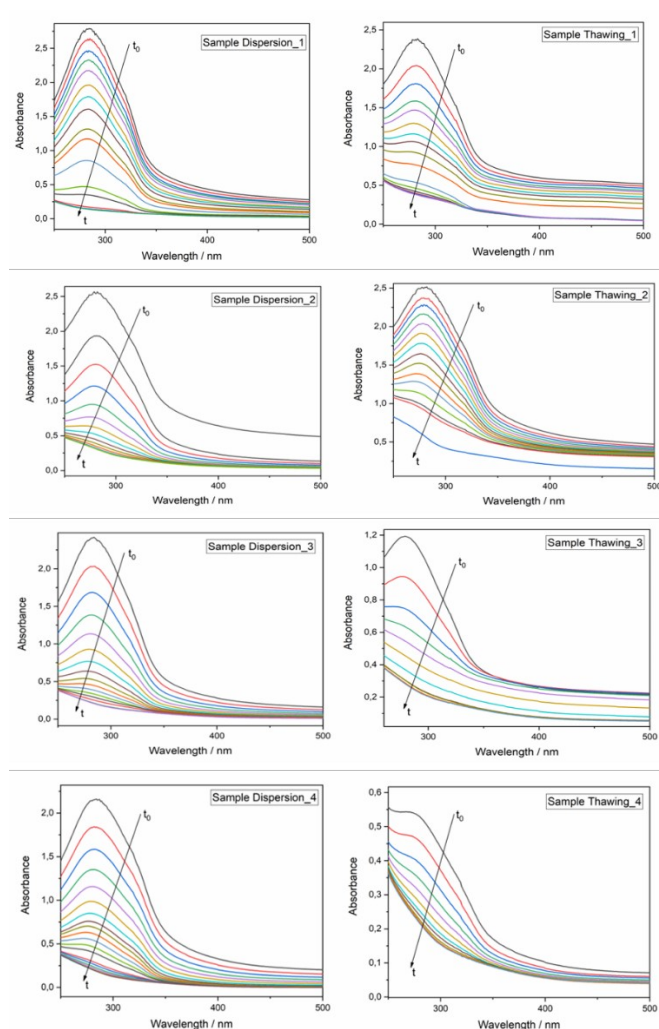


**Fig. S6.** UV-Vis spectra for NPs **1 – 4** immediately after sample dispersion in H<sub>2</sub>O (left) and sample thawing from -20 °C to RT (right).



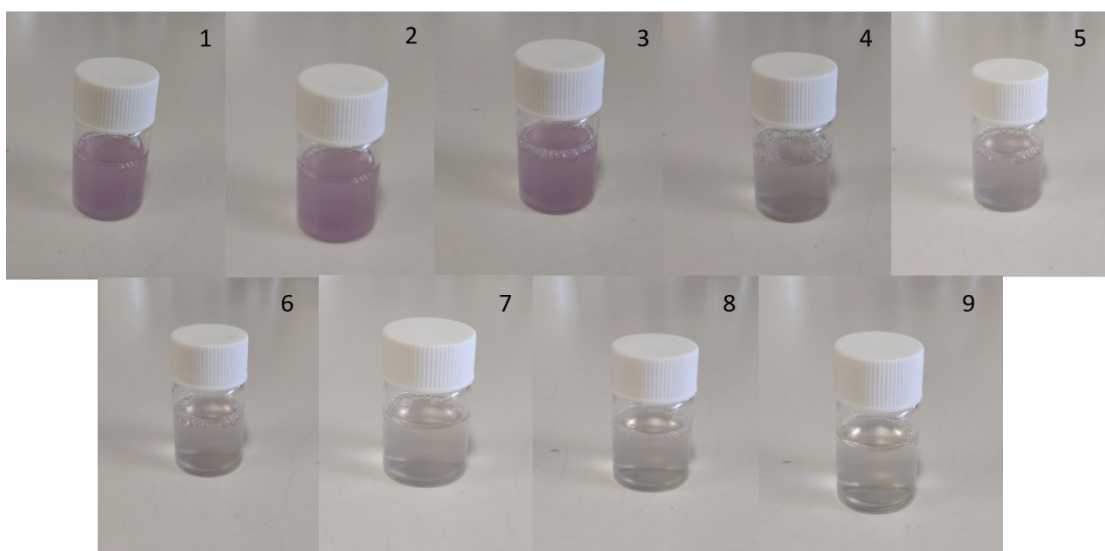


**Fig. S7.** Gradual color change (purple 1 → colorless 9) for the NPs immediately after sample dispersion in H<sub>2</sub>O at RT.

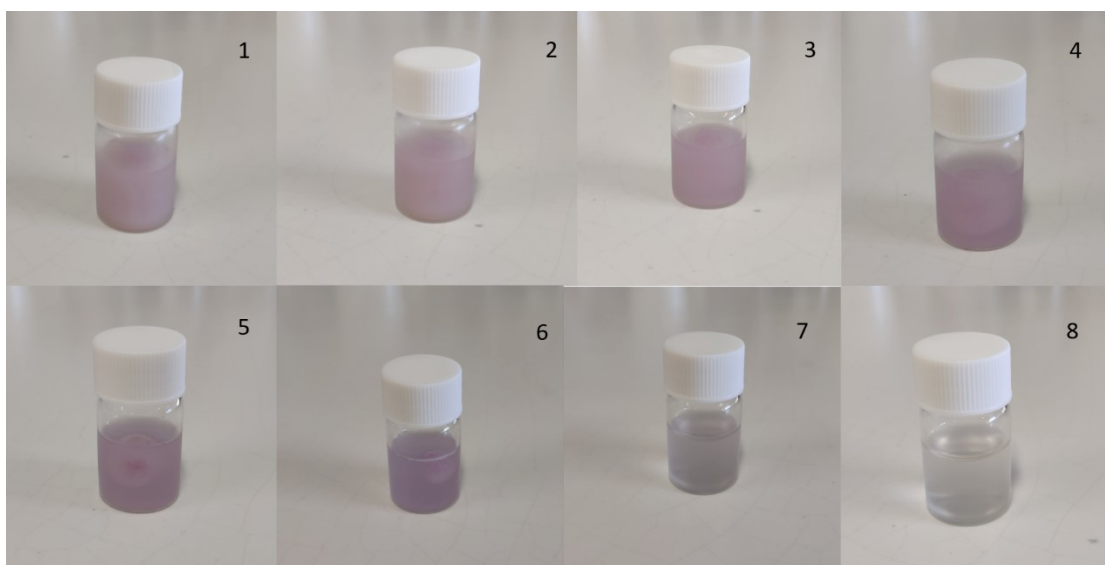


**Fig. S8.** Gradual color change (1 purple → 8 colorless) for the NPs during sample thawing from -20 °C to RT.

## Dynamic Light Scattering

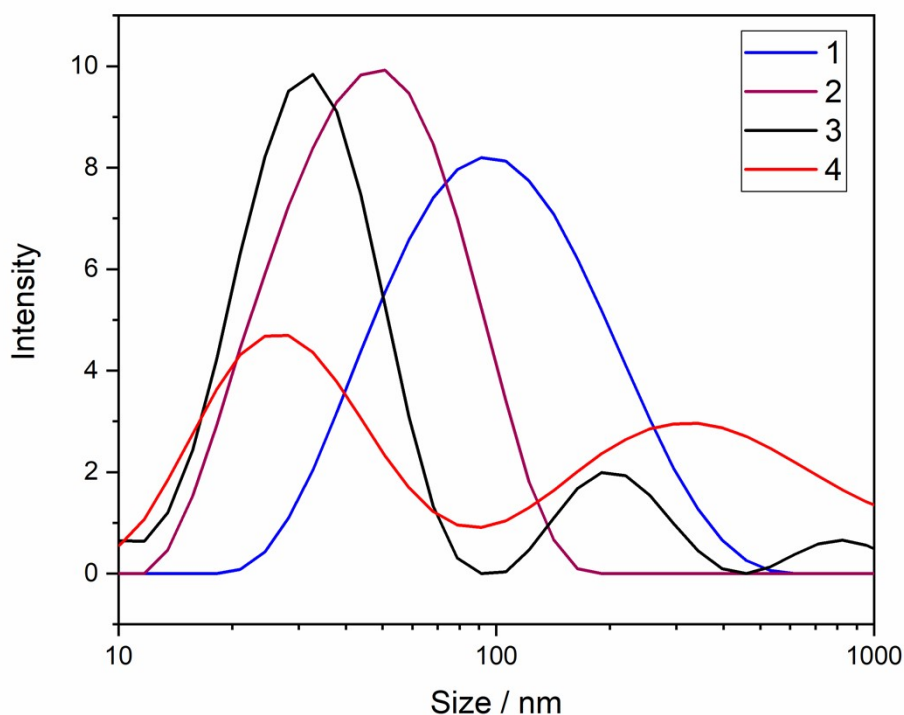


**Fig. S9.** DLS measurements for NPs **1 – 4** in aqueous dispersion.

**Table S4.** Mean size of the NPs calculated by TEM and DLS techniques for solid state and aqueous dispersions, respectively.

<b>Samples</b>	<b>Size of the NPs calculated by TEM</b>	<b>Size of the dispersed NPs calculated by DLS</b>	<b>Zeta Potential</b>
<b>1</b>	50 nm	100 nm	34 mV
<b>2</b>	10 nm	50 nm	39 mV
<b>3</b>	25 nm	30 nm	36 mV
<b>4</b>	25 nm	25 nm	31 mV

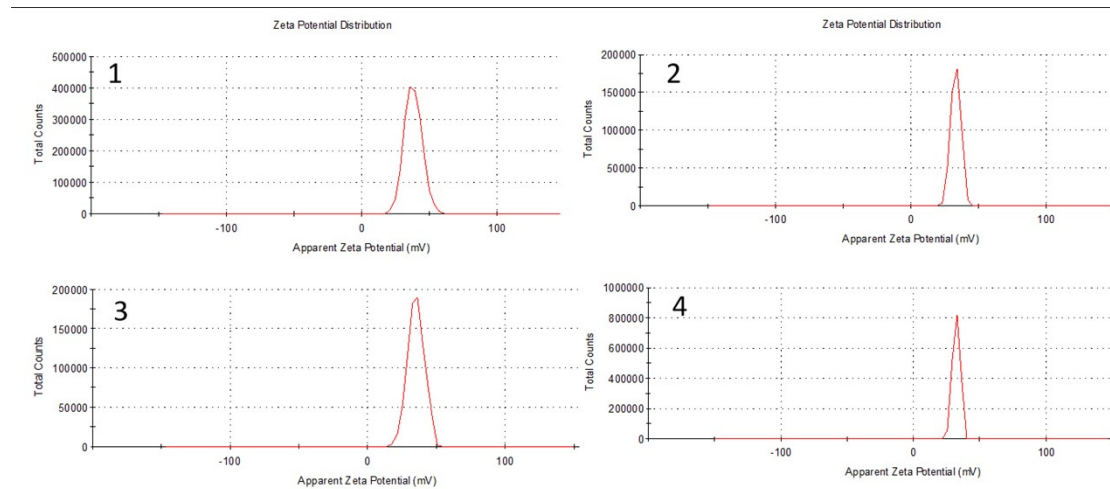


**Fig. S10.** Zeta potential distribution curve for aqueous dispersions of NPs **1 - 4**.

# Differential Scanning Calorimetry

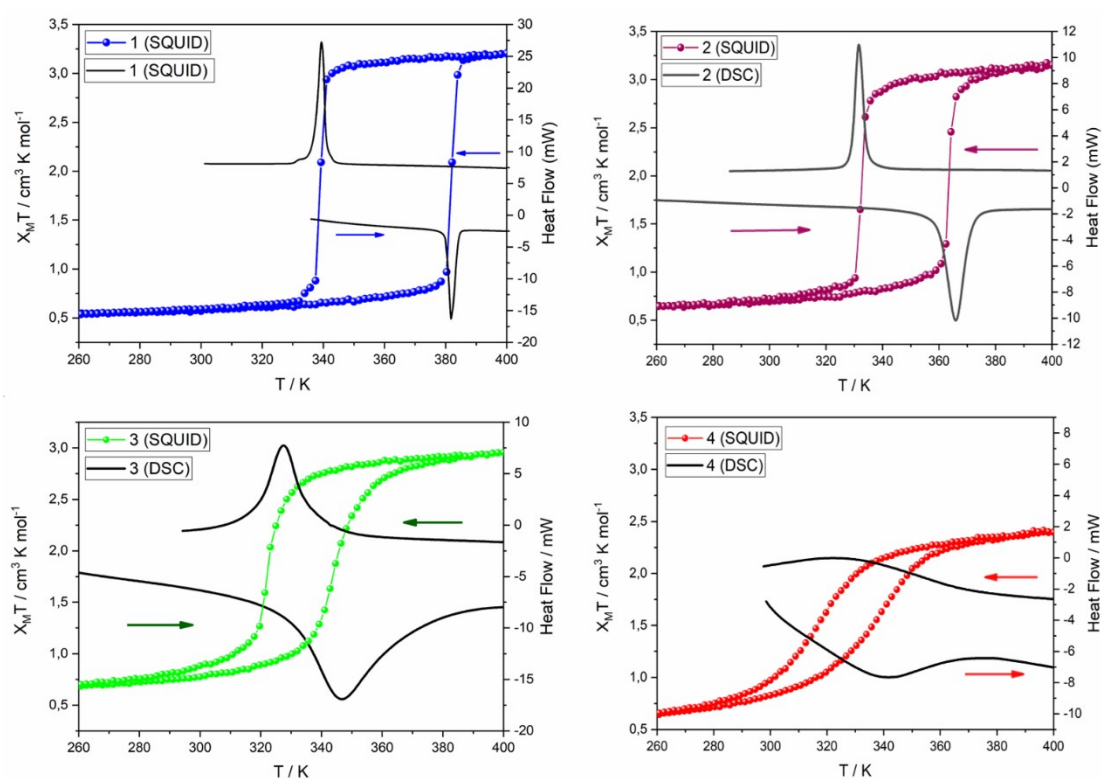


**Fig. S11.** Thermal dependence of the  $\chi_{MT}$  product and DSC analysis for NPs **1 - 4** with scan rate 1 K/min.

**Table S5.** Magnetic parameters derived from thermal susceptibility measurements of the NPs **1 – 4** and the lyophilized analogues.

NPs	$T_{inc} \uparrow$ (K)	$T_{decr} \downarrow$ (K)	$\Delta T$	$\chi_{MT}$ ( $\text{cm}^3 \text{K mol}^{-1}$ )
1	382	339	43	3.06
1-lyoph	333	309	24	2.00
2	366	332	34	2.29
2-lyoph	328	312	16	2.29
3	345	322	23	2.69
3-lyoph	323	299	24	1.53
4	338	318	20	2.60
4-lyoph	322	298	24	2.34

# Magnetic Resonance Imaging

## Custom-built phantom

All tubes were placed in a custom-built phantom consisting of a plastic container filled with water, a 3mm thick silicone tray to absorb vibrations during scanning and immobilize the 16-place polypropylene tube rack in the water bath (Fig. S12). Temperature control was performed through a valve which released water from the container, while hot water was manually added when needed depending on frequent temperature measurements using a probe type digital thermometer. A removable lid covered the opening of the container maintaining a temperature range of  $\pm 1^{\circ}\text{C}$ .

## Imaging Protocol

All measurements were performed on a 3.0 T MRI scanner (GE Healthcare, Signa HDx, Milwaukee, WI, USA) using a neurovascular array 8-channel head coil. 2D images for T1 relaxation time calculations were acquired using an inversion recovery (IR) spin-echo pulse sequence with echo time (TE) 1.6ms, repetition time (TR) 3000ms, slice thickness 5mm, flip angle  $90^{\circ}$  and matrix size  $256 \times 256$ . Inversion time (TI) ranged from 50ms to 3000ms (50, 100, 200, 300, 400, 500, 600, 700, 800, 900, 1000, 1100, 1200, 1300, 1400, 1500, 1750, 2000, 2250, 2500, 2750 και 3000ms).

T2 relaxation curves were obtained by a single-echo spin-echo sequence with repetition time (TR) 1500ms, slice thickness 5mm, flip angle  $90^{\circ}$  and matrix size  $512 \times 512$ . Echo time (TE) ranged from 15ms to 300ms (15, 35, 55, 75, 95, 115, 135, 155, 175, 190, 200, 225, 250, 275 and 300ms).

A set of seven contrast agent solutions (NPs 1 in concentrations 0.964, 1.93, 3.86 and 7.72 mM and NPs 2 in concentrations 1.07, 2.13 and 4.27 mM) were scanned to measure T2 relaxation times at 20, 30 and 40  $^{\circ}\text{C}$  and a set of two contrast agent solutions (NPs 3: 3.85 mM and NPs 4: 3.76 mM) were scanned to calculate both longitudinal (T1) and transverse (T2) relaxation times including relaxation times of distilled water (solvent) at 20, 30, 40 and 50  $^{\circ}\text{C}$ .

## Calculation of Relaxation Times

T1 and T2 relaxation curves were extracted from a semi-automated custom-designed MATLAB code to improve measurement reproducibility. Same size ROIs (region of interest) were placed on axial images of the samples within each tube, excluding the tube wall and susceptibility artifacts (Fig. S13). Matrices of signal intensity (SI) and standard deviation (std) at different TEs, TIs and temperatures were generated for each contrast agent solution.

$R_1$  relaxation rate ( $R_1=1/T_1$ ) was determined using a MATLAB (R2020a) Curve Fitting Toolbox to fit SI versus TI curve to a 3-parameter fitting model defined by the following equation (1).

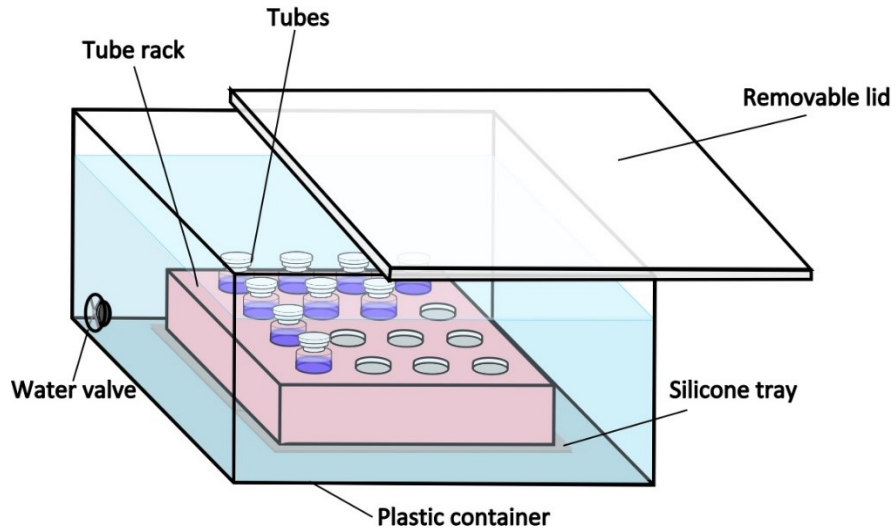


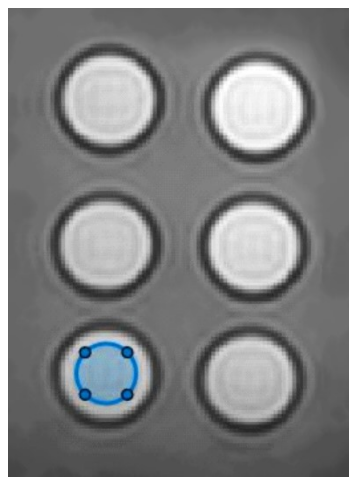
**Fig. S12.** Custom-built phantom

$$SI(TI) = A + B \cdot e^{-\frac{TI}{T_1}} \quad (\text{eq. 1})$$

$R_2$  relaxation rates ( $R_2=1/T_2$ ) were calculated in like manner, fitting SI versus TE curve to the following 3-parameter curve fitting equation (2) [2]:

$$SI(TE) = C + D \cdot e^{-\frac{TE}{T_2}} \quad (\text{eq. 2})$$

The uncertainty of  $R_1$  and  $R_2$  were described by the fitting errors.



## Calculation of Relaxivities

Relaxivity ( $r_{1,2}$ ) is the ability of a contrast media to enhance protons relaxation rate [3] and was calculated from equation (3),

$$R_{1,2} = R_{1,2}^0 + r_{1,2} \cdot C \quad (\text{eq. 3})$$

where  $R_2$  is the transverse relaxation rate of a solution containing contrast agent,  $R_2^0$  the relaxation rate of the solvent without the presence of contrast agent and  $C$  the concentration

**Fig. S13.** FROI placement, MATLAB semi-automated code

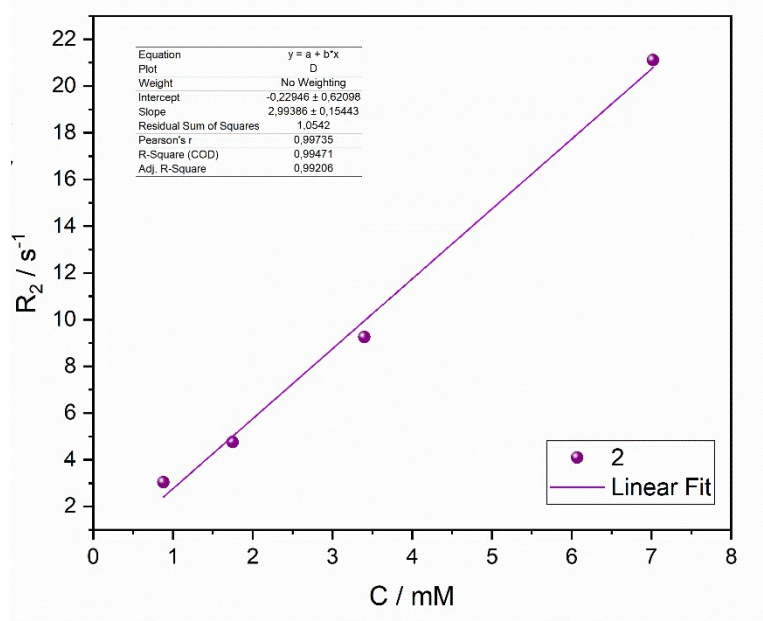


**Fig. S14.** Graphic determination of  $r_2$  for NPs **2** at 3T in water. Plot of relaxation rate  $R_2$  versus concentration and their linear regression at 30 °C.

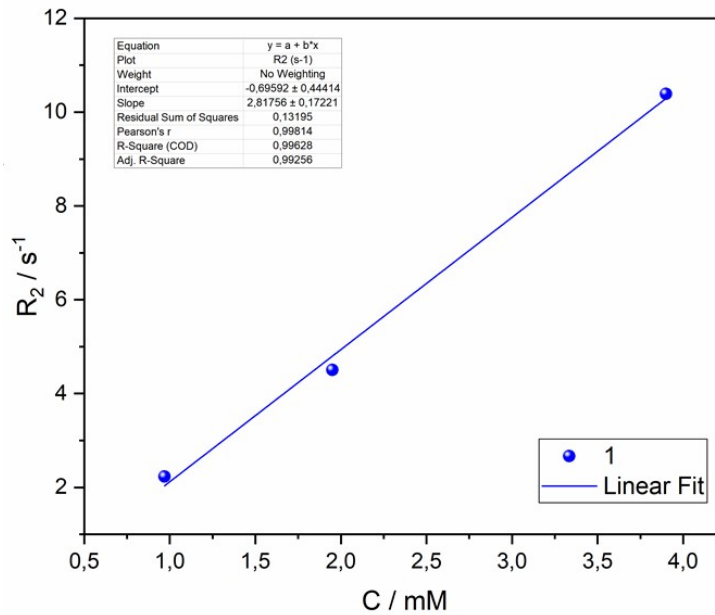


**Fig. S15.** Graphic determination of  $r_2$  for NPs **1** at 3T in water. Plot of relaxation rate  $R_2$  versus concentration and their linear regression at 30 °C.

Relaxivity  $r_2$  was calculated as the slope of the linear regression of the plot  $R_2$  (Figs S14 and S15) versus concentration separately for each contrast agent.  $R_2$  relaxation rate was measured in three different concentrations (0.97, 1.95 and 3.9 mM) for NPs **1** and in four different concentrations (0.88, 1.75, 3.40 and 7.02 mM) for NPs **2**. A concentration with a value close to 3.00 mM was considered as the preferable concentration for NPs **3-4** considering the efficiency of a contrast agent as a combination of the relaxation rate  $R_2$  and the concentration. T2-w image of the phantom is depicted for NPs **1** and **2** in Fig. S16 showing the concentration dependence of the contrast after the use of different concentrations and echo (TE) times. T1 and T2-w images are also depicted in Figs. S17 & S18 for NPs **3** and **4** at 20°C and 50°C in various inversion (TI) and echo (TE) times.

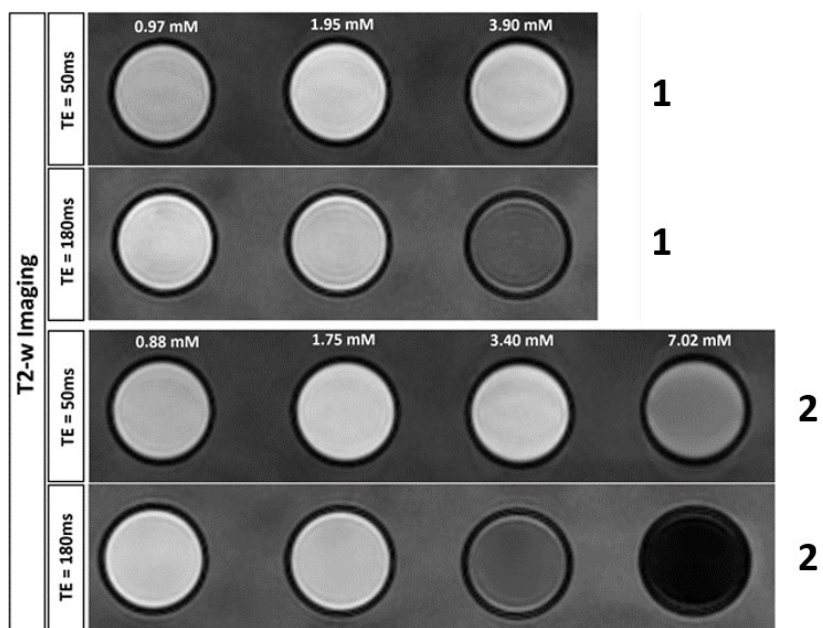


**Fig. S16.** T2-w images of **1** and **2** in different concentrations (increasing from left to right) for TE=50 ms and TE=180 ms.

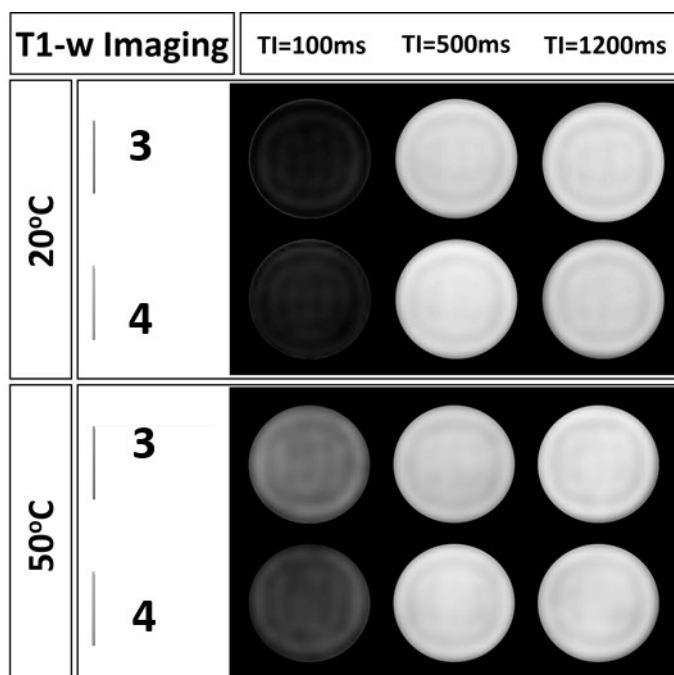


**Fig. S17.** T1-w images of **3** and **4** at 20 °C and 50 °C for TI (inversion time) = 100, 500 and 1200 ms.

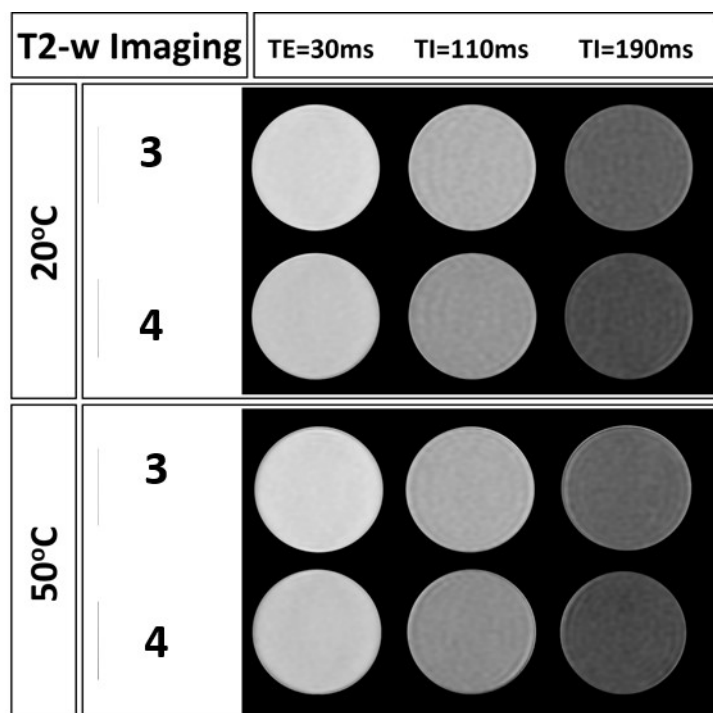


**Fig. S18.** T2-w images of **3** and **4** at 20 °C and 50 °C for TE (echo time) = 30, 110 and 190 ms.

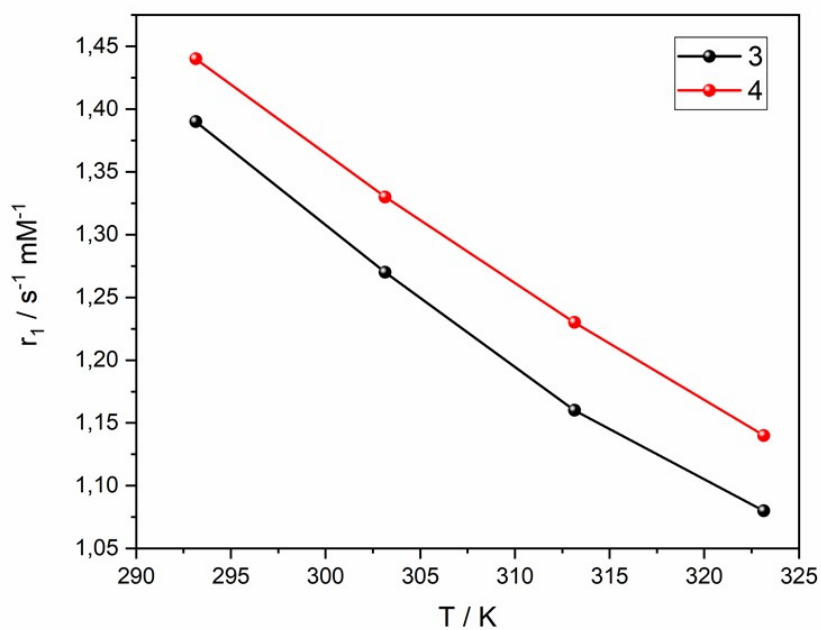


**Fig. S19.** Thermal dependence of  $r_1$  relaxivity for NPs **3** and **4**.

## References

- 1 M. Rohrer, H. Bauer, J. Mintorovitch, M. Requardt and H. J. Weinmann, *Invest Radiol.*, 2005, **40**, 715.
- 2 Y. Shen, F. L. Goerner, C. Snyder, J. N. Morelli, D. Hao, D. Hu, X. Li and V. M. Runge, *Invest Radiol.*, 2015, **50**, 330.
- 3 Y. Shen, F. L. Goerner, J. T. Heverhagen, C. Snyder, D. Hu, X. Li and V. M. Runge, *Acta Radiol.*, 2019, **60**, 694.
- 4 A. Bjørnerud, *The Physics of Magnetic Resonance Imaging FYS-KJM 4740* [Internet]. Oslo; 2008.